A SURVEY OF CURRENT METHODS IN MEDICAL IMAGE SEGMENTATION

Dzung L. Pham*†, Chenyang Xu*, Jerry L. Prince*

* Department of Electrical and Computer Engineering,
The Johns Hopkins University, Baltimore MD 21218
† Laboratory of Personality and Cognition,
GRC/NIA/NIH, 5600 Nathan Shock Dr., Baltimore, MD 21224

Technical Report JHU/ECE 99-01

Submitted for publication to
Annual Review of Biomedical Engineering
January 19, 1998

Total number of pages: 27

A Survey of Current Methods in Medical Image Segmentation

Dzung L. Pham[*†], *Chenyang Xu*[*], *Jerry L. Prince*[*]

[*] Department of Electrical and Computer Engineering, The Johns Hopkins University
3400 N. Charles St. Baltimore, MD 21218

[†] Laboratory of Personality and Cognition, National Institute on Aging
5600 Nathan Shock Dr., Baltimore, MD 21224

KEYWORDS: medical imaging, image processing, classification, deformable models, magnetic resonance imaging

ABSTRACT: Image segmentation plays a crucial role in many medical imaging applications by automating or facilitating the delineation of anatomical structures and other regions of interest. We present herein a critical appraisal of the current status of semi-automated and automated methods for the segmentation of anatomical medical images. Current segmentation approaches are reviewed with an emphasis placed on revealing the advantages and disadvantages of these methods for medical imaging applications. The use of image segmentation in different imaging modalities is also described along with the difficulties encountered in each modality. We conclude with a discussion on the future of image segmentation methods in biomedical research.

1 Introduction

Diagnostic imaging is an invaluable tool in medicine today. Magnetic resonance imaging (MRI), computed tomography (CT), digital mammography, and other imaging modalities provide an effective means for noninvasively mapping the anatomy of a subject. These technologies have greatly increased knowledge of normal and diseased anatomy for medical research and are a critical component in diagnosis and treatment planning.

With the increasing size and number of medical images, the use of computers in facilitating their processing and analysis has become necessary. In particular, computer algorithms for the delineation of anatomical structures and other regions of interest are a key component in assisting and automating specific radiological tasks. These algorithms, called *image segmentation* algorithms, play a vital role in numerous biomedical imaging applications such as the quantification of tissue volumes [98], diagnosis [176], localization of pathology [208], study of anatomical structure [198], treatment planning [90], partial volume correction of functional imaging data [128], and computer-integrated surgery [6, 61].

Methods for performing segmentations vary widely depending on the specific application, imaging modality, and other factors. For example, the segmentation of brain tissue has different requirements from the segmentation of the liver. General imaging artifacts such as noise, partial volume effects, and motion can also have significant consequences on the performance of segmentation algorithms. Furthermore, each imaging modality has its own idiosyncrasies with which to contend. There is currently no single segmentation method that yields acceptable results for every medical image. Methods do exist

that are more general and can be applied to a variety of data. However, methods that are specialized to particular applications can often achieve better performance by taking into account prior knowledge. Selection of an appropriate approach to a segmentation problem can therefore be a difficult dilemma.

This chapter provides an overview of current methods used for computer assisted or computer automated segmentation of anatomical medical images. Methods and applications that have appeared in the recent literature are briefly described. A full description of competing methods is beyond the scope of this chapter and the readers are referred to references for additional details. We focus instead on providing the reader an introduction to the different applications of segmentation in medical imaging and the various issues that must be confronted. Also, we refer only to the most commonly used radiological modalities for imaging anatomy: magnetic resonance imaging (MRI), X-ray computed tomography (CT), ultrasound, and X-ray projection radiography. Most of the concepts described, however, are applicable to other imaging modalities as well.

This chapter is organized as follows. In Section 2, common terminology and issues associated with the segmentation of medical images are defined and discussed. In Section 3, we briefly describe methodologies used in common segmentation approaches. In Section 4, we review the ways in which segmentation methods have recently been applied in different imaging modalities. Finally in Section 5, important issues relating to the future of medical image segmentation are discussed.

2 Background

In this section we define terminology that will be used throughout and describe important issues in the segmentation of medical images.

2.1 Definitions

An image is a collection of measurements in two-dimensional (2-D) or three-dimensional (3-D) space. In medical images, these measurements or *image intensities* can be radiation absorption in X-ray imaging, acoustic pressure in ultrasound, or RF signal amplitude in MRI. If a single measurement is made at each location in the image, then the image is called a *scalar* image. If more than one measurement is made (eg. dual-echo MRI), the image is called a vector or *multi-channel* image. Images may be acquired in the continuous domain such as on X-ray film, or in discrete space as in MRI. In 2-D discrete images, the location of each measurement is called a *pixel* and in 3-D images, it is called a *voxel*. For simplicity, we will often use the term "pixel" to refer to both the 2-D and 3-D cases.

Classically, image segmentation is defined as the partitioning of an image into non-overlapping, constituent regions which are homogeneous with respect to some characteristic such as intensity or texture [66, 59, 132]. If the domain of the image is given by I, then the segmentation problem is to determine the sets $S_k \subset I$ whose union is the entire image I. Thus, the sets that make up a segmentation must satisfy

$$I = \bigcup_{k=1}^{K} S_k \tag{1}$$

where $S_k \bigcap S_j = \emptyset$ for $k \neq j$, and each S_k is connected. Ideally, a segmentation method finds those sets that correspond to distinct anatomical structures or regions of interest in the image.

When the constraint that regions be connected is removed, then determining the sets S_k is called *pixel classification* and the sets themselves are called *classes.* Pixel classification rather than classical segmentation is often a desirable goal in medical images, particularly when disconnected regions belonging to the same tissue class need to be identified. Determination of the total number of classes K in pixel classification can be a difficult problem [97]. Often, the value of K is assumed to be known based on prior knowledge of the anatomy being considered.

Labeling is the process of assigning a meaningful designation to each region or class and can be performed separately from segmentation. It maps the numerical index k of set S_k, to an anatomical designation. In medical imaging, the labels are often visually obvious and can be determined upon inspection by a physician or technician. Computer automated labeling is desirable when labels are not obvious and in automated processing systems. A typical situation involving labeling occurs in digital mammography where the image is segmented into distinct regions and the regions are subsequently labeled as being healthy tissue or tumorous.

Methods which delineate a structure or structures in an image, including both classical segmentation and pixel classification methods, are considered in this review. Although we do not discuss specific labeling methods, we will discuss several techniques that perform both segmentation and labeling simultaneously.

Two fields closely related to segmentation that we do not discuss here are feature detection and motion estimation. The distinction we make between segmentation and feature detection is that feature detection is concerned with determining the presence of some image property while segmentation generally assumes that the property is already present and attempts to precisely localize areas that possess the property. For example, edge detection methods can determine the location of edges in an image but without further processing, do not necessarily extract any region of interest. Motion estimation methods often consist of applying segmentation algorithms to time sequences of images. We consider this application of segmentation to be a separate branch of research and do not include it in this review.

2.2 Dimensionality

Dimensionality refers to whether a segmentation method operates in a 2-D image domain or a 3-D image domain. Methods that rely solely on image intensities are independent of the image domain. However, certain methods such as deformable models, Markov random fields, and region growing (described in Section 3), incorporate spatial information and may therefore operate differently depending on the dimensionality of the image. Generally, 2-D methods are applied to 2-D images and 3-D methods are applied to 3-D images. In some cases, however, 2-D methods are applied sequentially to the slices of a 3-D image [7, 52, 103, 141]. This may arise because of practical reasons such as ease of implementation, lower computational complexity, and reduced memory requirements. In addition, certain structures are more easily defined along 2-D slices.

A unique situation that occurs in medical image segmentation is the delineation of regions on a non-Euclidean domain, such as in brain cortex parcellation [148, 156]. This is essentially segmentation on a *surface* of measurements. Because a surface is a 2-D object folded in 3-D space, segmentation on a surface can not be treated as a standard 2-D or 3-D problem. The modeling of spatial characteristics along a surface is much more difficult than in a standard imaging plane because of the irregular sampling used by mesh representations and because of the need to compute geodesics [89]. This is an emerging area of research and preliminary results have shown great promise.

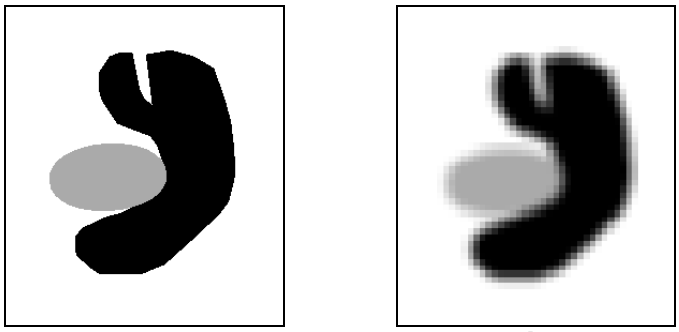

(a) (b)

Figure 1: Illustration of partial volume effect: (a) Ideal image, (b) acquired image.

2.3 Soft segmentation and partial volume effects

Segmentations that allow regions or classes to overlap are called *soft segmentations.* Soft segmentations are important in medical imaging because of *partial volume effects*, where multiple tissues contribute to a single pixel or voxel resulting in a blurring of intensity across boundaries. Figure 1 illustrates how the sampling process can result in partial volume effects, leading to ambiguities in structural definitions. In Figure 1b, it is difficult to precisely determine the boundaries of the two objects. A *hard segmentation* forces a decision of whether a pixel is inside or outside the object. Soft segmentations on the other hand, retain more information from the original image by allowing for uncertainty in the location of object boundaries. Note that the point spread function of an imaging device can be larger than the spatial extent of a single pixel or voxel. Thus, partial volume effects can cause boundaries to be blurred across significant portions of an image.

In pixel classification methods, the notion of a soft segmentation stems from the generalization of a set *characteristic function.* A characteristic function is simply an indicator function of where a pixel is inside or outside its corresponding set. For a location $j \in I$, the characteristic function $\chi_k(j)$ of the set S_k is defined to be

$$\chi_k(j) = \begin{cases} 1 & \text{if } j \in S_k \\ 0 & \text{otherwise} \end{cases} \tag{2}$$

Characteristic functions can be generalized to *membership functions* [205] which need not be binary valued. Membership functions $m_k(j)$ satisfy the following constraints:

$$0 \leq m_k(j) \leq 1, \text{ for all } k, j \tag{3}$$

$$\sum_{k=1}^{K} m_k(j) = 1, \text{ for all } j \tag{4}$$

The value of a membership function $m_k(j)$ can be interpreted as the contribution of class k to location j. Thus, wherever membership values are greater than zero for two or more classes, those classes are overlapping. Conversely, if the membership function is unity for some value of j and k, then class k is the only contributing class at location j. Membership functions can be derived using fuzzy clustering and classifier algorithms [140, 71], statistical algorithms in which case the membership functions are probability functions [106, 197], or they can be computed as estimates of partial volume fractions

[24]. Soft segmentations based on membership functions can be easily converted to hard segmentations by assigning a pixel to its class with the highest membership value.

2.4 Continuous or discrete segmentations

Nearly all medical images used for image segmentation are represented as discrete samples on a uniform grid. Segmentation methods typically operate on the same discrete grid as the image. However, certain methods such as deformable models (see Section 3.7) are capable of operating in the continuous spatial domain, thereby providing the potential for subpixel accuracy in delineating structures. Subpixel accuracy is desirable particularly when the resolution of the image is on the same order of magnitude as the structure of interest.

Segmentation on the continuous domain is not equivalent to partial volume estimation or other soft segmentation methods. Partial volume estimation methods merely provide the fraction of a structure which is present in a voxel. This may be sufficient for quantification purposes but not in situations where precise localization is required, such as for tumors in surgical or radiotherapy planning. Continuous segmentation methods actually reconstruct how a structure passes through a voxel. Although continuous segmentation methods have subpixel or subvoxel resolution, their precision and accuracy are still dependent on the resolution of the original data. Furthermore, this level of precision can be difficult to validate on real data.

2.5 Interaction

The tradeoff between manual interaction and performance is an important consideration in any segmentation application. Manual interaction can improve accuracy by incorporating prior knowledge of an operator. However, for large population studies, this can be laborious and time consuming.

The type of interaction required by segmentation methods can range from completely manual delineation of an anatomical structure, to the selection of a seed point for a region growing algorithm (see Section 3.2). The differences in these types of interaction are the amount of time and effort required, as well as the amount of training required by an operator. Methods that rely on manual interaction can also be vulnerable to reliability issues. However, even "automated" segmentation methods typically require some interaction for specifying initial parameters that can significantly affect performance.

2.6 Validation

In order to quantify the performance of a segmentation method, validation experiments are necessary. Validation is typically performed using one of two different types of truth models. The most straightforward approach to validation is by comparing the automated segmentations with manually obtained segmentations (cf. [199, 186]). This approach, besides suffering from the drawbacks outlined in the previous section, does not guarantee a perfect truth model since an operator's performance can also be flawed. The other common approach to validating segmentation methods is through the use of physical phantoms [102] or computational phantoms [36]. Physical phantoms provide an accurate depiction of the image acquisition process but typically do not present a realistic representation of anatomy. Computational phantoms can be more realistic in this latter regard, but simulate the image acquisition process using only simplified models.

Once a truth model is available, a figure of merit must be defined for quantifying accuracy or precision (cf. [20]). The choice of the figure of merit is dependent on the application and can be based on region information such as the number of pixels misclassified, or boundary information such as distance to the true boundary. A survey on this topic is provided in [206].

3 Methods

In this section, we briefly describe several common approaches that have appeared in the recent literature on medical image segmentation. We define each method, provide an overview of how the method is implemented, and discuss its advantages and disadvantages. Although each technique is described separately, multiple techniques are often used in conjunction with one another for solving different segmentation problems.

We divide segmentation methods into eight categories: (1) thresholding approaches, (2) region growing approaches, (3) classifiers, (4) clustering approaches, (5) Markov random field models, (6) artificial neural networks, (7) deformable models, and (8) atlas-guided approaches. Other notable methods that do not belong to any of these categories are described at the end of this section. Of the methods discussed in this section, thresholding, classifier, clustering, and Markov random field approaches can be considered pixel classification methods.

Most of the image segmentation methods that we will describe can be posed as optimization problems where the desired segmentation minimizes some energy or cost function defined by the particular application. In probabilistic methods, this is equivalent to maximizing a likelihood or *a posteriori* probability. Given the image $\mathbf{y}$, we desire the segmentation $\hat{\mathbf{x}}$ such that

$$\hat{\mathbf{x}} = \arg\min_{\mathbf{x}} \mathcal{E}(\mathbf{x}, \mathbf{y}) \tag{5}$$

where $\mathcal{E}$, the energy function, depends on the observed image $\mathbf{y}$ and a segmentation $\mathbf{x}$. Defining an appropriate $\mathcal{E}$ is a major difficulty in designing segmentation algorithms because of the wide variety of image properties that can be used, such as intensity, edges, and texture. In addition to information derived from the image, prior knowledge can also be incorporated to further improve performance. The advantage of posing a segmentation as an optimization problem is that it precisely defines what is desirable in the segmentation. It is clear that for different applications, different energy functions are necessary.

Several general surveys on image segmentation exist in the literature [66, 132]. Additional surveys on image segmentation specifically for medical images have also appeared [21, 11, 172, 208, 29, 6].

3.1 Thresholding

Thresholding approaches segment scalar images by creating a binary partitioning of the image intensities. Figure 2a shows the histogram of a scalar image that possesses three apparent classes corresponding to the three modes. A thresholding procedure attempts to determine an intensity value, called the *threshold*, which separates the desired classes. The segmentation is then achieved by grouping all pixels with intensity greater than the threshold into one class, and all other pixels into another class. Two potential thresholds are shown in Figure 2a at the valleys of the histogram. Determination of more than one threshold value is a process called multithresholding [155].

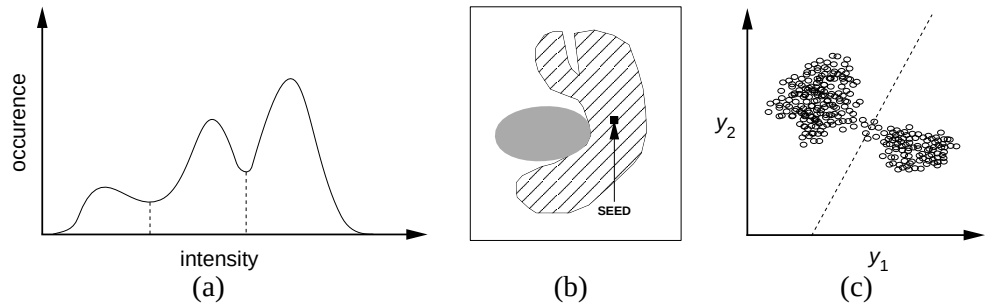

(a) (b) (c)

Figure 2: Feature space methods and region growing: (a) a histogram showing three apparent classes, (b) a 2-D feature space, (c) example of region growing.

Thresholding is a simple yet often effective means for obtaining a segmentation in images where different structures have contrasting intensities or other quantifiable features. The partition is usually generated interactively, although automated methods do exist [155]. For scalar images, interactive methods can be based on an operator's visual assessment of the resulting segmentation since the thresholding operation is implementable in real-time.

Thresholding is often used as an initial step in a sequence of image processing operations. Its main limitations are that in its simplest form only two classes are generated and it can not be applied to multi-channel images. In addition, thresholding typically does not take into account the spatial characteristics of an image. This causes it to be sensitive to noise and intensity inhomogeneities, which can occur in magnetic resonance images (see Section 4.2). Both these artifacts essentially corrupt the histogram of the image, making separation more difficult. For these reasons, variations on classical thresholding have been proposed for medical image segmentation that incorporate information based on local intensities [104] and connectivity [99]. A survey on thresholding techniques is provided in [155].

3.2 Region growing

Region growing is a technique for extracting a region of the image that is connected based on some predefined criteria. This criteria can be based on intensity information and/or edges in the image [66]. In its simplest form, region growing requires a seed point that is manually selected by an operator, and extracts all pixels connected to the initial seed with the same intensity value. This is depicted in Figure 2b, where region growing has been used to isolate one of the structures from Figure 1a.

Like thresholding, region growing is not often used alone but within a set of image processing operations, particularly for the delineation of small, simple structures such as tumors and lesions [57, 143]. Its primary disadvantage is that it requires manual interaction to obtain the seed point. Thus, for each region that needs to be extracted, a seed must be planted. Split and merge algorithms are related to region growing but do not require a seed point [115]. Region growing can also be sensitive to noise, causing extracted regions to have holes or even become disconnected. Conversely, partial volume effects can cause separate regions to become connected. To help alleviate these problems, a homotopic region growing algorithm has been proposed that preserves the topology between an initial region and an extracted region [114]. Fuzzy analogies to region growing have also been developed [183].

3.3 Classifiers

Classifier methods are pattern recognition techniques that seek to partition a feature space derived from the image using data with known labels [159, 11]. A *feature space* is the range space of any function of the image, with the most common feature space being the image intensities themselves. A histogram, as shown in Figure 2a, is an example of a 1-D feature space. Figure 2c shows an example of a partitioned 2-D feature space with two apparent classes. All pixels with their associated features on the left side of the partition would be grouped into one class. Although the features used can be related to texture or other properties, we assume for simplicity that the features are simply intensity values.

Classifiers are known as *supervised* methods since they require training data that are manually segmented and then used as references for automatically segmenting new data. There are a number of ways in which training data can be applied in classifier methods. A simple classifier is the nearest-neighbor classifier, where each pixel or voxel is classified in the same class as the training datum with the closest intensity. The k-nearest-neighbor (kNN) classifier is a generalization of this approach, where the pixel is classified according to the majority vote of the k closest training data. The kNN classifier is considered a nonparametric classifier since it makes no underlying assumption about the statistical structure of the data. Another nonparametric classifier is the Parzen window, where the classification is made according to the majority vote within a predefined window of the feature space centered at the unlabeled pixel intensity.

A commonly-used parametric classifier is the maximum likelihood (ML) or Bayes classifier. It assumes that the pixel intensities are independent samples from a mixture of probability distributions, usually Gaussian. This mixture, called a finite mixture model, is given by the probability density function

$$f(y_j;\theta,\pi) = \sum_{k=1}^{K} \pi_k f_k(y_j;\theta_k) \tag{6}$$

where y_j is the intensity of pixel j, f_k is a component probability density function parameterized by θ_k, and $\theta = [\theta_1,\ldots,\theta_K]$. The variables π_k are mixing coefficients that weight the contribution of each density function and $\pi = [\pi_1,\ldots,\pi_K]$. Training data is collected by obtaining representative samples from each component of the mixture model and then estimating each θ_k accordingly. For Gaussian mixtures, this means estimating K means, covariances, and mixing coefficients. Classification of new data is obtained by assigning each pixel to the class with the highest posterior probability. When the data truly follows a finite Gaussian mixture distribution, the ML classifier can perform well and is capable of providing a soft segmentation composed of the posterior probabilities. Additional parametric and nonparametric classifiers are described in [208].

Standard classifiers require that the structures to be segmented possess distinct quantifiable features. Because training data can be labeled, classifiers can transfer these labels to new data as long as the feature space sufficiently distinguishes each label as well. Being non-iterative, they are relatively computationally efficient and unlike thresholding methods, they can be applied to multi-channel images. A disadvantage of classifiers is that they generally do not perform any spatial modeling. This weakness has been addressed in recent work extending classifier methods to segmenting images that are corrupted by intensity inhomogeneities [197]. Neighborhood and geometric information were also incorporated into a classifier approach in [85]. Another disadvantage is the requirement of manual interaction for obtaining training data. Training sets can be

acquired for each image that requires segmenting, but this can be time consuming and laborious. On the other hand, use of the same training set for a large number of scans can lead to biased results which do not take into account anatomical and physiological variability between different subjects.

3.4 Clustering

Clustering algorithms essentially perform the same function as classifier methods without the use of training data. Thus, they are termed *unsupervised* methods. In order to compensate for the lack of training data, clustering methods iterate between segmenting the image and characterizing the properties of the each class. In a sense, clustering methods train themselves using the available data.

Three commonly used clustering algorithms are the K-means or ISODATA algorithm [34], the fuzzy c-means algorithm [46, 11], and the expectation-maximization (EM) algorithm [102, 107]. The K-means clustering algorithm clusters data by iteratively computing a mean intensity for each class and segmenting the image by classifying each pixel in the class with the closest mean [75]. Figure 3b shows the result of applying the K-means algorithm to a slice of a MR brain image in Figure 3a. The number of classes was assumed to be three, representing (from dark gray to white) cerebrospinal fluid, gray matter, and white matter. The fuzzy c-means algorithm generalizes the K-means algorithm [11], allowing for soft segmentations based on fuzzy set theory [205]. The EM algorithm applies the same clustering principles with the underlying assumption that the data follows a Gaussian mixture model (see Eq. (6)). It iterates between computing the posterior probabilities and computing maximum likelihood estimates of the means, covariances, and mixing coefficients of the mixture model.

Although clustering algorithms do not require training data, they do require an initial segmentation (or equivalently, initial parameters). The EM algorithm has demonstrated greater sensitivity to initialization than the K-means or fuzzy c-means algorithms [42]. Like classifier methods, clustering algorithms do not directly incorporate spatial modeling and can therefore be sensitive to noise and intensity inhomogeneities. This lack of spatial modeling, however, can provide significant advantages for fast computation [69]. Work on improving the robustness of clustering algorithms to intensity inhomogeneities in MR images has demonstrated excellent success [58, 140]. Robustness to noise can be incorporated using Markov random field modeling as described in the next section.

3.5 Markov random field models

Markov random field (MRF) modeling itself is not a segmentation method but a statistical model which can be used within segmentation methods. MRFs model spatial interactions between neighboring or nearby pixels. These local correlations provide a mechanism for modeling a variety of image properties [105]. In medical imaging, they are typically used to take into account the fact that most pixels belong to the same class as their neighboring pixels. In physical terms, this implies that any anatomical structure that consists of only one pixel has a very low probability of occurring under a MRF assumption.

MRFs are often incorporated into clustering segmentation algorithms such as the K-means algorithm under a Bayesian prior model [133, 149, 70, 58]. The segmentation is then obtained by maximizing the *a posteriori* probability of the segmentation given the image data using iterative methods such as iterated conditional modes [10] or simulated annealing [54]. Figure 3c, shows the robustness to noise in a segmentation resulting

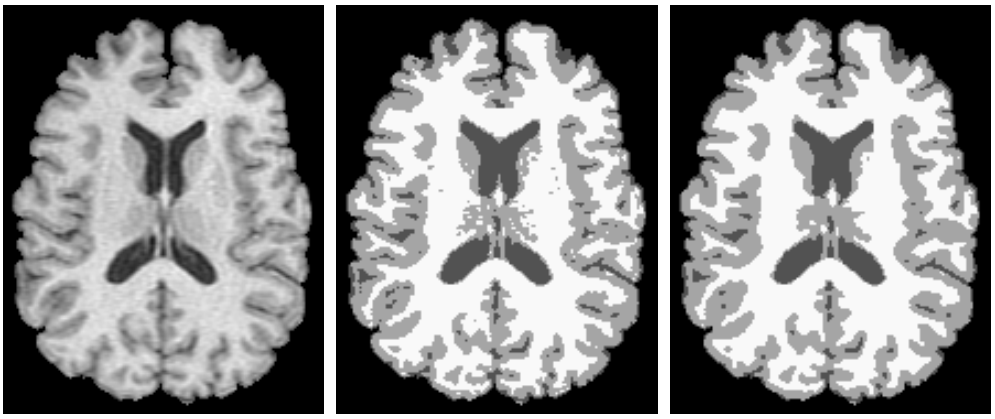

(a) (b) (c)

Figure 3: Segmentation of a MR brain image: (a) original image, (b) segmentation using the K-means algorithm, (c) segmentation using the K-means algorithm with a Markov random field prior.

from an MRF prior. The segmentation is much smoother than the non-MRF result of Figure 3b.

A difficulty associated with MRF models is proper selection of the parameters controlling the strength of spatial interactions [105]. Too high a setting can result in an excessively smooth segmentation and a loss of important structural details. In addition, MRF methods usually require computationally intensive algorithms. Despite these disadvantages, MRFs are widely used not only to model segmentation classes, but also to model intensity inhomogeneities that can occur in MR images [70] and texture properties [153].

3.6 Artificial neural networks

Artificial neural networks (ANNs) are massively parallel networks of processing elements or nodes that simulate biological learning. Each node in an ANN is capable of performing elementary computations. Learning is achieved through the adaptation of weights assigned to the connections between nodes. A thorough treatment on neural networks can be found in [27, 68].

ANNs represent a paradigm for machine learning and can be used in a variety of ways for image segmentation. The most widely applied use in medical imaging is as a classifier [64, 53], where the weights are determined using training data, and the ANN is then used to segment new data. ANNs can also be used in an unsupervised fashion as a clustering method [11, 152], as well as for deformable models [191].

Because of the many interconnections used in a neural network, spatial information can easily be incorporated into its classification procedures. Although ANNs are inherently parallel, their processing is usually simulated on a standard serial computer, thus reducing this potential computational advantage.

3.7 Deformable models

Deformable models are physically motivated, model-based techniques for delineating region boundaries using closed parametric curves or surfaces that deform under the in-

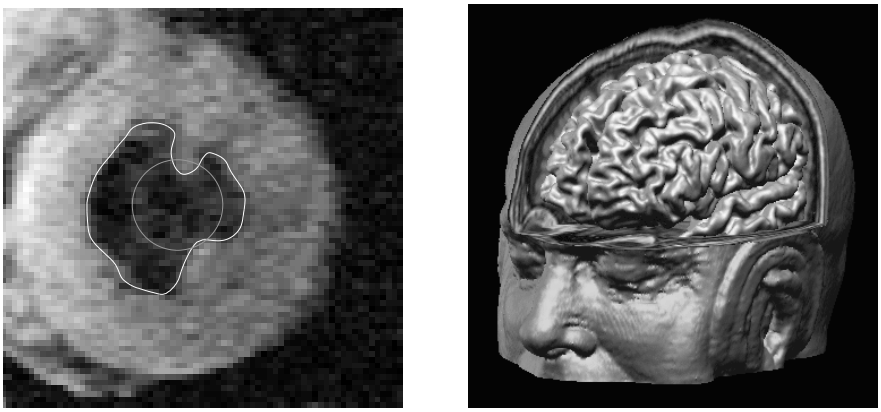

(a) (b)

Figure 4: (a) A 2-D example of using a deformable contour to extract the inner wall of the left ventricle of a human heart from an MR image. The initial deformable contour (plotted in gray) and the final converged result (plotted in white). (b) A 3-D example of using a deformable surface to reconstruct the brain cortical surface from a 3-D MR image.

fluence of internal and external forces. To delineate an object boundary in an image, a closed curve or surface must first be placed near the desired boundary and then allowed to undergo an iterative relaxation process. Internal forces are computed from within the curve or surface to keep it smooth throughout the deformation. External forces are usually derived from the image to drive the curve or surface towards the desired feature of interest. Figure 4a shows an example of applying a 2-D deformable model or *active contour* to a MR heart image. The active contour was initialized as a circle, and then allowed to deform to the inner boundary of the left ventricle. Figure 4b shows an example of a 3-D deformable surface that was used to extract the cerebral cortex from a MR head scan.

Mathematically, a deformable model moves according to its dynamic equations and seeks the minimum of a given energy functional [87, 180]. The deformation of a typical 2-D deformable model can be characterized by the following dynamic equation:

$$\mu(s)\frac{\partial^2 \mathbf{x}(s,t)}{\partial t^2} + \gamma(s)\frac{\partial \mathbf{x}(s,t)}{\partial t} = \mathbf{F}_{\text{int}} + \mathbf{F}_{\text{ext}} \tag{7}$$

where $\mathbf{x}(s,t) = (x(s,t), y(s,t))$ is a parametric representation of the position of the model at a given time t, and $\mu(s)$ and $\gamma(s)$ are parameters representing the mass density and damping density of the model, respectively. Eq. (7) causes the model to move according to the direction and magnitude of the forces on the right hand side. The most commonly used internal forces are

$$\mathbf{F}_{\text{int}} = \frac{\partial}{\partial s}\left(\alpha(s)\frac{\partial \mathbf{x}(s,t)}{\partial s}\right) - \frac{\partial^2}{\partial s^2}\left(\beta(s)\frac{\partial^2 \mathbf{x}}{\partial s^2}\right) \tag{8}$$

which represent internal stretching and bending forces. The most commonly used external forces are computed as the gradient of an edge map (as shown in Figure 4b).

The main advantages of deformable models are their ability to directly generate closed parametric curves or surfaces from images and their incorporation of a smoothness constraint that provides robustness to noise and spurious edges. A disadvantage is that they

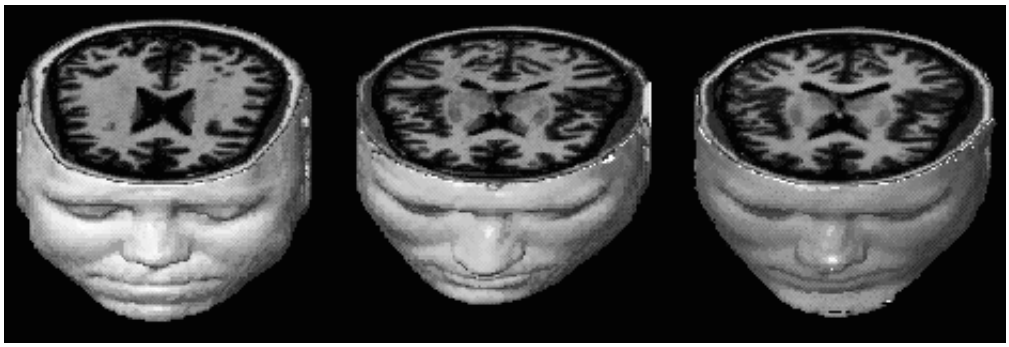

(a) (b) (c)

Figure 5: Demonstration of atlas warping: (a) template image, (b) target image, (c) warped template (Images provided courtesy of G.E. Christensen and M.I. Miller).

require manual interaction to place an initial model and choose appropriate parameters. Reducing sensitivity to initialization has been a topic of research that has demonstrated excellent success [33, 18, 112, 201]. Standard deformable models can also exhibit poor convergence to concave boundaries. This difficulty can be alleviated somewhat through the use of pressure forces [33] and other modified external force models [201]. Another important extension of deformable models is the adaptivity of model topology using an implicit representation rather than an explicit parameterization [18, 112, 118]. A general review on deformable models in medical image analysis can be found in [119].

3.8 Atlas-guided approaches

Atlas-guided approaches are a powerful tool for medical image segmentation when a standard atlas or template is available. The atlas is generated by compiling information on the anatomy that requires segmenting. This atlas is then used as a reference frame for segmenting new images. Conceptually, atlas-guided approaches are similar to classifiers except they are implemented in the spatial domain of the image rather than in a feature space.

The standard atlas-guided approach treats segmentation as a registration problem (see [111] for a detailed survey on registration techniques). It first finds a one-to-one transformation that maps a pre-segmented atlas image to the target image that requires segmenting. This process is often referred to as *atlas warping.* The warping can be performed using linear [175, 96, 151] transformations but because of anatomical variability, a sequential application of linear and non-linear [35, 39, 26, 156] transformations is often used. An example of atlas warping for a MR head scan is shown in Figure 5 [26]. Because the atlas is already segmented, all structural information is transferred to the target image. This is shown in Figure 6, where the Talairach brain atlas [175] has been mapped to an MR image [39].

Atlas-guided approaches have been applied mainly in MR brain imaging. An advantage of atlas-guided approaches is that labels are transferred as well as the segmentation. They also provide a standard system for studying morphometric properties [41, 181, 79]. Even with non-linear registration methods however, accurate segmentations of complex structures is difficult due to anatomical variability. This is shown in Figure 6 where the cerebral cortex is not segmented as accurately as shown in Figure 3. Thus, atlas-guided

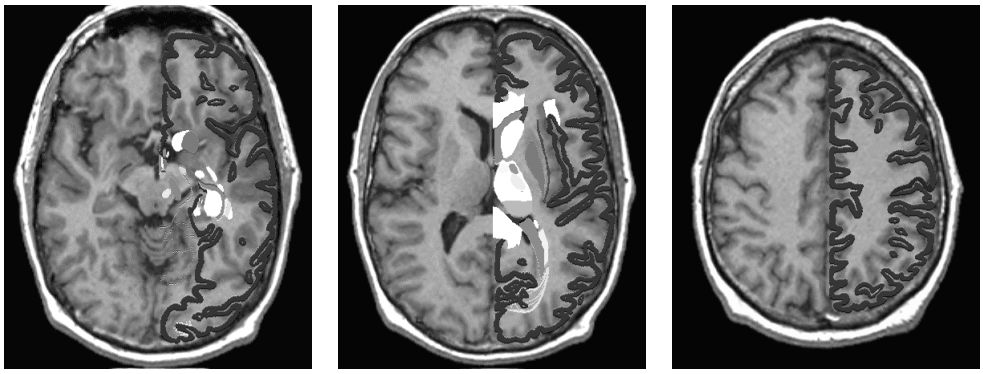

Figure 6: Three slices from a MR brain volume overlaid with a warped atlas (Images provided courtesy of C.A. Davatzikos).

approaches are generally better-suited for segmentation of structures that are stable over the population of study. One method that helps model anatomical variability is the use of probabilistic atlases [181] but these require additional time and interaction to accumulate data.

3.9 Other approaches

Model-fitting is a segmentation method that typically fits a simple geometric shape such as an ellipse or parabola to the locations of extracted image features in an image [137]. It is a technique which is specialized to the structure being segmented but is easily implemented and can provide good results when the model is appropriate. A more general approach is to fit spline curves or surfaces [7] to the features. The main difficulty with model-fitting is that image features must first be extracted before the fitting can take place.

The watershed algorithm uses concepts from mathematical morphology [59] to partition images into homogeneous regions [192]. This method can suffer from oversegmentation, which occurs when the image is segmented into an unnecessarily large number of regions. Thus, watershed algorithms in medical imaging are usually followed by a postprocessing step to merge separate regions that belong to the same structure [161].

4 Modalities

In this section, we review the application of segmentation to various medical imaging modalities. We describe the specific issues relevant to each modality and the anatomical regions for which segmentation methods have been applied. For information about the physics behind the image acquisition process in these modalities, see [110, 170].

4.1 Magnetic resonance imaging

The majority of research in medical image segmentation pertains to its use for MR images, especially in brain imaging. This is because of MR's ability to provide a combination of high resolution (on the order of 1mm cubic voxels), excellent soft tissue contrast, and a high signal-to-noise ratio. Furthermore, multi-channel MR images with varying contrast characteristics can be acquired, providing additional information for

distinguishing between different structures. For general reviews on the segmentation of MR images, see [11, 139, 106, 208, 29]. Direct comparisons of different methods for segmenting MR images are also available [187, 30, 64].

Because of its ability to derive contrast from a number of tissue parameters, many different pulse sequences exist for acquiring MR images. Determining the optimal pulse sequence for obtaining accurate segmentations [147] is therefore an important problem that requires knowledge of the underlying tissue properties of the anatomy to be segmented [141, 50]. Furthermore, because of the anatomical and physiological variability between different subjects, different populations may require different pulse sequences [141].

Much of the literature on segmentation in MRI focuses specifically on the segmentation of head scans in normal subjects. There are three general goals in this application: 1) extract the brain volume, 2) segment brain tissue into gray matter, white matter, and cerebrospinal fluid, and 3) delineate specific brain structures such as the cerebral cortex or the hippocampus. An exception to this categorization is the use of atlas-guided methods [35], which are capable of fully segmenting and labeling all structures of the brain simultaneously, but also have certain disadvantages (see Section 3.8). Overviews on the segmentation of neuroanatomy are provided in [32, 198].

Brain volume extraction is a difficult problem in MR head scans, particularly in T1-weighted images. However, it is often a necessary step before segmentation of other structures can take place. Problems in brain volume extraction arise because there is a great deal of overlap in intensity values between the non-brain and brain tissues and because the two can often appear connected. One method to deal with these difficulties is to allow for some loss of brain tissue in a preliminary segmentation step and then to recover the tissue using morphological filters [16, 156]. Several methods have also applied deformable models as a final step in a sequence of image processing operations [84, 1, 5]. Atlas-guided approaches have also been applied [1].

Methods that attempt to segment brain tissue as gray matter, white matter, and cerebrospinal fluid use either T1-weighted scalar data [77, 126, 72, 122, 149, 194] or multispectral data [189, 108, 24, 91, 55, 64, 30, 107, 67, 88, 182, 152]. The trend in the literature has been favoring the use of T1-weighted data which is capable of providing higher resolution data without increasing acquisition time and still maintaining good tissue contrast and low noise. Classifier approaches [17, 197, 85], clustering approaches [64, 107, 140], neural network approaches [64, 152], and Markov random fields [70, 149] have all been used for brain segmentation. Because most of these methods are based on intensity information, a major concern is the presence of intensity inhomogeneities, a topic discussed in the next section. Because the gray matter in the brain is thin and highly convoluted, partial volume effects are another important consideration. Efforts in modeling partial volume effects have used statistical methods [24, 157, 158, 17, 76, 95], soft segmentation derived through fuzzy set theory [28, 13, 154, 140], and linear filters [166].

The automated segmentation of specific structures in brains is an important area of research for morphometric analysis. Segmentation of the cerebral cortex has received much attention with most methods employing deformable models [52, 40, 120, 178, 200]. Deformable models have also been used for segmenting a variety of other structures such as the ventricles [116, 195], the corpus callosum [41, 195], the hippocampus [4, 56], and others [173, 190, 177]. Although not often employed for segmenting the cortex, atlas-guided methods also appear well-suited for segmenting subcortical brain structures such as the ventricles [2, 142] and the hippocampus [79]. Segmentation of tumors and lesions in the brain has been applied to magnetic resonance images using

neural networks [207], atlas-guided approaches [83], linear filters [166], fuzzy region growing [185], and deformable models [19]. Because of its complexity, this problem typically requires a sequence of operators [196, 57].

Besides head scans, segmentation has also been used for extracting a variety of other structures. Segmentation in cardiac imaging has been used for delineating the cavities of the left ventricle using region growing and thresholding approaches [163, 44], as well as deformable models [12, 145, 9]. Deformable models in cardiac imaging, however, are more often proposed for tracking motion in the heart [8]. Markov random field models have been used for segmenting knee images [25] as well as magnetic resonance angiograms (MRAs) [188]. Other methods for segmenting MRAs include deformable models [109] and thresholding [31]. Although MRA does not require catheterization, segmentation in standard angiography is more common because of its generally superior contrast and spatial and temporal resolution [168, 48, 65, 47].

4.2 Intensity inhomogeneities in MRI

A major difficulty in the segmentation of MR images is the intensity inhomogeneity artifact [162, 37, 164], which causes a shading effect to appear over the image. This artifact can significantly degrade the performance of methods that assume that the intensity value of a tissue class is constant over the image. Figure 7a shows an axially acquired MR image of a female heart with myocardial infarction. Intensity inhomogeneities are noticeable particular near the breast areas. Numerous approaches have been proposed in the literature for performing tissue classification in the presence of intensity inhomogeneity artifacts. Some methods suggest a prefiltering operation that attempts to remove the inhomogeneity prior to actual segmentation [108, 43, 123, 76, 100, 92, 14, 165]. Methods that *simultaneously* segment the image while estimating the inhomogeneity however, offer the advantage of being able to use intermediate information gained from the segmentation.

There are two prevailing approaches for modeling inhomogeneities in methods that perform simultaneous segmentation. The first approach assumes that the mean tissue intensity for each tissue class is spatially varying and independent of one another [133, 202, 149, 130]. The second approach models the inhomogeneities as a multiplicative gain field [150, 140] or additive bias field of the image logarithm [197, 62, 70, 85]. It is unclear which of these two provides more accurate modeling of inhomogeneity effects, although the second approach has the advantage of being computationally less expensive. The second approach can also be used for removing inhomogeneities by simple multiplication of the acquired image by the reciprocal of the estimated gain field. Figure 7 shows the results of applying the adaptive fuzzy c-means algorithm that performs a soft segmentation while compensating for intensity inhomogeneities [140]. The heart image was segmented into three classes and Figure 7d-f correspond to the membership functions for those three classes. Figure 7b shows the gain field estimated from the original image. The hard segmentation in Figure 7c was obtained as outlined in Section 2.3. Note that the ring artifact present in Figure 7e results from partial volume effects causing the boundary between fat, skin, and air to have an intensity similar to that of muscle. This effect is common and a disadvantage of intensity-based pixel classification methods.

4.3 Chest radiography

Chest radiographs have not received much recent attention in the segmentation literature partly because the projection nature of the images makes quantification and localization

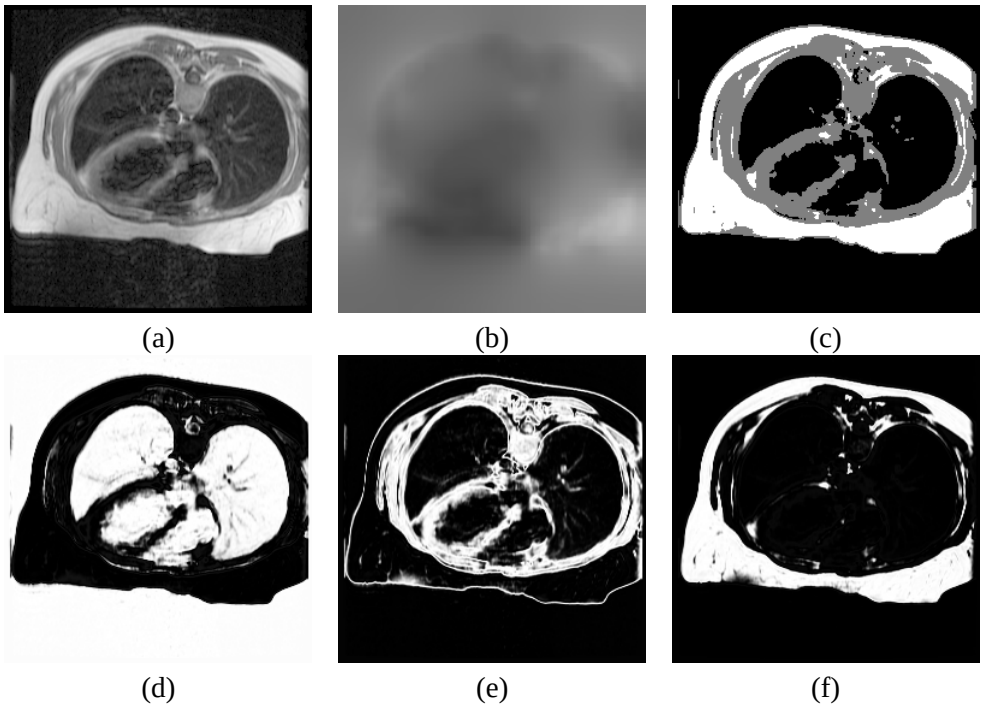

Figure 7: Example of simultaneous inhomogeneity correction and soft segmentation: (a) MR heart image acquired using a fast spin echo sequence in a true axial prescription, (b) estimated gain field, (c) hard segmentation into three classes, (d)-(f) membership functions of the three classes (Data provided courtesy of C. Constantinides).

a difficult task and also because their analysis often does not require a segmentation . Despite these issues, efforts have been made for segmenting chest radiographs into anatomical regions using classifiers [121, 193] and Markov random fields [193]. In addition, an algorithm has been proposed for delineating posterior rib borders using active contour models [204].

4.4 Computed tomography

X-ray computed tomography (CT) alleviates some of the difficulties associated with projection radiography and allows for 3-D imaging at resolutions equal to or better than MRI. Soft tissue contrast in CT is not as good as in MRI, but CT remains the modality of choice for imaging bone and bone tumors. Segmentation of bone can be achieved using thresholding and region growing operations [60] as well as more sophisticated methods such as Markov random fields [135], deformable models [134, 177, 145, 129], and fuzzy region growing [183]. Once segmented, image renderings are often used to provide detailed visualization of skeletal structure [184].

Segmentation in CT has also been applied to thoracic scans using statistical clustering [102], a combination of region growing and watershed algorithms [199], a combination of region growing and fuzzy logic [15], and deformable models [174, 78, 145]. Some methods have been applied specifically for the reconstruction of bronchial trees [167, 136]. CT images have also been used in brain segmentation [103], although MR imaging is presently more common in neuroimaging segmentation applications. In ad-

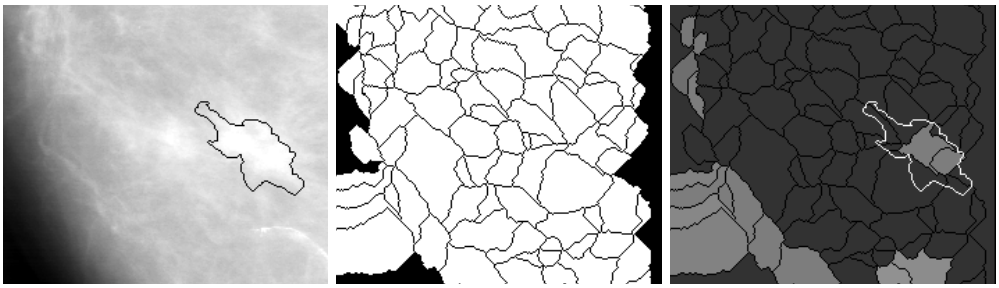

(a) (b) (c)

Figure 8: Segmentation in digital mammography: (a) digitized mammogram and radiologist's boundary for biopsy-proven malignant tumor, (b) result of watershed algorithm, (c) suspicious regions determined by automated method (Images provided courtesy of C.E. Priebe).

dition, liver segmentation has been performed using model-fitting [7], and deformable models [116, 49, 127, 56]. Deformable models have also been applied in other CT segmentation applications, including the delineation of abdominal aortic aneurysms [80], segmentation of the stomach [113], and segmentation of the heart [117, 78, 160].

4.5 Digital mammography

Segmentation in digital mammography is typically performed for localization of tumors [143, 103], microcalcification clusters [23, 74, 171], or other indicators of pathology [82]. In delineating suspicious masses for mammography, segmentation methods are typically employed in one of two ways. In the first approach, the mammogram is initially segmented into candidate regions which are then labeled as being suspicious or normal [144, 104, 74, 86]. In the second approach, the image is first processed to detect for the presence of pathology and a segmentation is performed as a final step to determine its precise location [23, 94, 63, 22]. Thresholding and its variations are the most often used segmentation technique in mammography [144, 171, 23, 63, 74], although extensions of region growing methods have also been proposed [94, 143]. A comparison of thresholding and region growing was presented in [82]. Because pathological areas often possess different textural properties in mammograms, Markov random field methods have also been successfully employed [104, 22].

Figure 8 shows an example where the mammogram is initially oversegmented using a watershed algorithm. A statistical classifier [146] is then used to determine which regions contain microcalcifications. This classification step is typically performed using textural properties. As illustrated in the figure, false positives can be a significant problem in the detection of suspicious masses in mammograms (although in this case, they fall outside the breast area). For these reasons, computer automated detection in mammography has been used only as an aid to increase the reliability of a physician's diagnosis. Improved initial segmentations may lead to a reduction in false-positives. Note also that a perfect delineation of masses is difficult but not often necessary in mammography since detection is the primary goal.

4.6 Ultrasound

Segmentation algorithms have had fairly limited application in ultrasound imaging. High levels of speckling present in ultrasound images make accurate segmentations difficult. Furthermore, the real-time acquisition in ultrasound makes it better suited for motion estimation tasks (cf. [45, 124]) where active contours, because of their dynamic nature, are often used. Ultrasound is also often employed in detecting pathology using textural classifiers (cf. [125, 81]) but regions of interest are typically obtained through manual interaction.

Nevertheless, some automated segmentation work has been performed in ultrasound for extracting a variety of structures. In [179], a thresholding of intensity and texture statistics was used to segment ovarian cysts. Deformable models have had good success in ultrasound applications such as in the segmentation of echocardiograms [38, 160, 78, 93]. In [101], an active contour was used to determine the boundary of the calcaneus in broadband ultrasonic attenuation parameter images, which are less noisy than standard ultrasound images. In [19, 138], deformable models were used to determine the boundary of the fetus and the fetus head respectively. Deformable models have also been used to segment cysts in ultrasound breast images [203]. Other methods have been applied for the segmentation of coronary arteries in intravascular ultrasound images [169] and for segmenting the pubic arch in transrectal ultrasound [137].

4.7 Multimodal

Multimodal image segmentation attempts to take advantage of the different kinds of anatomical information provided by different imaging modalities. For example, multimodal imaging can take advantage of the bone imaging capabilities in CT and the soft tissue imaging capabilities in MRI. In brain imaging, functional imaging data can be used to help delineate tumors [29]. There are two major difficulties in multimodal image segmentation, however. First, multimodal data is not always available. Second, when the data is available, they are typically not in the same alignment, and therefore require registration [111]. Recent methods have been proposed for simultaneously registering and segmenting multimodal images [3]. Once the images have been registered, standard multi-channel segmentation techniques can be applied. Segmentation of multimodal images was targeted specifically in [131] using neural networks, and in [73], which presented a Bayesian framework for simultaneous restoration and segmentation.

5 Conclusion

Future research in the segmentation of medical images will strive towards improving the accuracy, precision, and computational speed of segmentation methods, as well as reducing the amount of manual interaction. Accuracy and precision can be improved by incorporating prior information from atlases and by combining discrete and continuous-based segmentation methods. For increasing computational efficiency, multiscale processing (cf. [51]) and parallelizable methods such as neural networks appear to be promising approaches. Computational efficiency will be particularly important in real-time processing applications.

Possibly the most important question surrounding the use of image segmentation is its application in clinical settings. Computerized segmentation methods have already demonstrated their utility in research applications and are now garnering increased use for computer aided diagnosis and radiotherapy planning. It is unlikely that automated

segmentation methods will ever replace physicians but they will likely become crucial elements of medical image analysis. Segmentation methods will be particularly valuable in areas such as computer integrated surgery, where visualization of the anatomy is a critical component.

Literature Cited

1. G.B. Aboutanos and B.M. Dawant. Automatic brain segmentation and validation: image-based versus atlas-based deformable models. In *Medical Imaging, SPIE Proc.*, volume 3034, pages 299–310, 1997.
2. L.K. Arata, A.P. Dhawan, J.P. Broderick, M.F. Gaskil-Shipley, A.V. Levy, and Nora D. Volkow. Three-dimensional anatomical model-based segmentation of MR brain images through principal axes registration. *IEEE T. Biomed. Eng.*, 42:1069–1078, 1995.
3. J. Ashburner and K. Friston. Multimodal image coregistration and partitioning– a unified framework. *Neuroimage*, 6:209–217, 1997.
4. E.A. Ashton, M.J. Berg, K.J. Parker, J. Weisberg, C.W. Chen, and L. Ketonen. Segmentation and feature extraction techniques, with applications to MRI head studies. *Mag. Res. Med.*, 33:670–677, 1995.
5. M.S. Atkins and B.T. Mackiewich. Fully automatic segmentation of the brain in MRI. *IEEE T. Med. Imag.*, 17:98–109, 1998.
6. N. Ayache, P. Cinquin, I. Cohen, L. Cohen, F. Leitner, and O. Monga. Segmentation of complex three-dimensional medical objects: a challenge and a requirement for computer-assisted surgery planning and performance. In R.H. Taylor, S. Lavallee, G.C. Burdea, and R. Mosges, editors, *Computer-integrated surgery: technology and clinical applications*, pages 59–74. MIT Press, 1996.
7. K.T. Bae, M.L. Giger, C. Chen, and C.E. Kahn. Automatic segmentation of liver structure in CT images. *Med. Phys.*, 20:71–78, 1993.
8. E. Bardinet, L.D. Cohen, and N. Ayache. Tracking and motion analysis of the left ventricle with deformable superquadrics. *Med. Im. Anal.*, 1:129–149, 1996.
9. E. Bardinet, L.D. Cohen, and N. Ayache. A parametric deformable model to fit unstructured 3D data. *Comp. Vis. Im. Understand.*, 71:39–54, 1998.
10. J. Besag. On the statistical analysis of dirty pictures. *CVGIP: Im. Understand.*, 57:359–372, 1986.
11. J.C. Bezdek, L.O. Hall, and L.P. Clarke. Review of MR image segmentation techniques using pattern recognition. *Med. Phys.*, 20:1033–1048, 1993.
12. D.C. Bloomgarden, Z.A. Fayad, V.A. Ferrari, B. Chin, M.G.S.J. Sutton, and L. Axel. Global cardiac function using fast breath-hold MRI: Validation of new acquisition and analysis techniques. *Magnetic Resonance in Medicine*, 37:683–692, 1997.
13. M.E. Brandt, T.P. Bohan, L.A. Kramer, and J.M. Fletcher. Estimation of CSF, white and gray matter volumes in hydrocephalic children using fuzzy clustering of MR images. *Computerized Medical Imaging and Graphics*, 18:25–34, 1994.
14. B.H. Brinkmann, A. Manduca, and R.A. Robb. Optimized homomorphic unsharp masking for MR grayscale inhomogeneity correction. *IEEE T. Med. Imag.*, 17:161–171, 1998.
15. M.S. Brown, M.F. McNitt-Gray, N.J. Mankovich, J.G. Goldin, J. Hiller, et al. Method for segmenting chest CT image data using an anatomical model: preliminary results. *IEEE T. Med. Imag.*, 16:828–839, 1997.
16. M.E. Brummer, R.M. Merseerau, R.L. Eisner, and R.R.J. Lewine. Automatic detection of brain contours in MRI data sets. *IEEE T. Med. Imag.*, 12:153–166, 1993.
17. E. Bullmore, M. Brammer, G. Rouleau, B. Everitt, A. Simmons, et al. Computerized brain tissue classification of magnetic resonance images: a new approach to the problem of partial volume artifact. *Neuroimage*, 2:133–147, 1995.
18. V. Caselles, F. Catte, T. Coll, and F. Dibos. A geometric model for active contours. *Numerische Mathematik*, 66:1–31, 1993.
19. V. Caselles, R. Kimmel, and G. Sapiro. Geodesic active contours. *Int. J. Comp. Vision*, 22:61–79, 1997.
20. V. Chalana and Y. Kim. A methodology for evaluation of boundary detection algorithms on medical images. *IEEE T. Med. Imag.*, 16:642–652, 1997.
21. E.L. Chaney and S.M. Pizer. Defining anatomical structures from medical images. *Seminars in Radiation Oncology*, 2:215–225, 1992.
22. C.H. Chen and G.G. Lee. On digital mammogram segmentation and microcalcification detection using multiresolution wavelet analysis. *Graph. Mod. Im. Proc.*, 59:349–364, 1997.

23. H. Cheng, Y.M. Lui, and R.I. Freimanis. A novel approach to microcalcification detection using fuzzy logic technique. *IEEE T. Med. Imag.*, 17:442–450, 1998.
24. H.S. Choi, D.R. Hanynor, and Y. Kim. Partial volume tissue classification of multichannel magnetic resonance images— a mixel model. *IEEE T. Med. Imag.*, 10:395–407, 1991.
25. S.M. Choi, J.E. Lee, J. Kim, and M.H. Kim. Volumetric objection reconstruction using the 3D-MRF model-based segmentation. *IEEE T. Med. Imag.*, 16:887–892, 1997.
26. G.E. Christensen, S.C. Joshi, and M.I. Miller. Volumetric transformation of brain anatomy. *IEEE T. Med. Imag.*, 16:864–877, 1997.
27. J.W. Clark. Neural network modelling. *Phys. Med. Biol.*, 36:1259–1317, 1991.
28. M.C. Clark, L.O. Hall, D.B. Goldgof, L.P. Clarke andR.P. Velthuizen, and M.S. Silbiger. MRI segmentation using fuzzy clustering techniques. *IEEE Eng. Med. Biol.*, pages 730–742, Nov/Dec 1994.
29. L.P. Clarke, R.P. Velthuizen, M.A. Camacho, J.J. Heine, M. Vaidyanathan, et al. MRI segmentation: methods and applications. *Mag. Res. Imag.*, 13:343–368, 1995.
30. L.P. Clarke, R.P. Velthuizen, S. Phuphanich, J.D. Schellenberg, J.A. Arrington, and M. Silbiger. MRI: stability of three supervised segmentation techniques. *Mag. Res. Imag.*, 11:95–106, 1993.
31. H.E. Cline, D.R. Thedens, P. Irarazaval, C.H. Meyer, B.S. Hu, D.G. Nishimura, and S. Ludke. 3-D MR coronary artery segmentation. *Mag. Res. Med.*, 40:697–702, 1998.
32. G. Cohen, N.C. Andreasen, R. Alliger, S. Arndt, J. Kuan, W.T.C. Yuh, and J. Er. Segmentation techniques for the classification of brain tissue using magnetic resonance imaging. *Psychiat.. Res.: Neuroimaging*, 45:33–51, 1992.
33. L.D. Cohen. On active contour models and balloons. *CVGIP: Image Understand.*, 53:211–218, 1991.
34. G.B. Coleman and H.C. Andrews. Image segmentation by clustering. *Proc. IEEE*, 5:773–785, 1979.
35. D.L. Collins, C.J. Holmes, T.M. Peters, and A.C. Evans. Automatic 3-D model-based neuroanatomical segmentation. *Human Brain Mapping*, 3:190–208, 1995.
36. D.L. Collins, A.P. Zijdenbos, V. Kollokian, J.G. Sled, N.J. Kabani, et al. Design and construction of a realistic digital brain phantom. *IEEE T. Med. Imag.*, 17:463–468, 1998.
37. B.R. Condon, J. Patterson, et al. Image non-uniformity in magnetic resonance imaging: its magnitude and methods for its correction. *The British Journal of Radiology*, 60:83–87, 1989.
38. G. Coppini, R. Poli, and G. Valli. Recovery of the 3-D shape of the left ventricle from echocardiographic images. *IEEE T. Med. Imag.*, 14:301–317, 1995.
39. C. Davatzikos. Spatial normalization of 3D images using deformable models. *J. Comp. Assist. Tom.*, 20:656–665, 1996.
40. C. Davatzikos and R.N. Bryan. Using a deformable surface model to obtain a shape representation of the cortex. *IEEE T. Med. Imag.*, 15:785–795, 1996.
41. C. Davatzikos, M. Vaillant, S. Resnick, J. L. Prince, S. Letovsky, and R. N. Bryan. A computerized method for morphological analysis of the corpus callosum. *J. Comp. Assist. Tom.*, 20:88–97, 1996.
42. J.W. Davenport, J.C. Bezdek, and R.J. Hathaway. Parameter estimation for finite mixture distributions. *Comput. Math. Applic.*, 15:810–828, 1988.
43. B.M. Dawant, A.P. Zijidenbos, and R.A. Margolin. Correction of intensity variations in MR images for computer-aided tissue classification. *IEEE T. Med. Imag.*, 12:770–781, 1993.
44. R. Deklerck, J. Cornelis, and M. Bister. Segmentation of medical images. *Im. Vis. Comp.*, 11:486–503, 1993.
45. J.M.B. Dias and J.M.N. Leitao. Wall position and thickness estimation from sequences of echocardiographic images. *IEEE T. Med. Imag.*, 15:25–38, 1996.
46. J.C. Dunn. A fuzzy relative of the ISODATA process and its use in detecting compact well-sparated clusters. *Journal of Cybernetics*, 3:32–57, 1973.
47. N. Ezquerra, S. Capell, L. Klein, and P. Duijves. Model-guided labeling of coronary structure. *IEEE T. Med. Imag.*, 17:429–441, 1998.
48. M.A.T. Figueiredo and J.M.N. Leitao. A nonsmoothing approach to the estimation of vessel contours in angiograms. *IEEE T. Med. Imag.*, 14:162–172, 1995.
49. E.K. Fishman, B.S. Kuszyk, D.G. Heath, L.M. Gao, and B. Cabral. Surgical planning for liver resection. *Computer*, 29:64–73, 1996.
50. L.M. Fletcher, J.B. Barsotti, and J.P. Hornak. A multispectral analysis of brain tissues. *Magn. Reson. Med.*, 29:623–630, 1993.
51. C.H. Fosgate, H. Krim, W.W. Irving, W.C. Karl, and A.S. Willsky. Multiscale segmentation and anomaly enhancement of SAR imagery. *IEEE T. Image Process.*, 6:7–20, 1997.
52. Y. Ge, J.M. Fitzpatrick, B.M. Dawant, J. Bao, R.M. Kessler, and R. Margolin. Accurate localization of cortical convolutions in MR brain images. *IEEE T. Med. Imag.*, 15:418–428, 1996.
53. E. Gelenbe, Y. Feng, and K.R.R. Krishnan. Neural network methods for volumetric magnetic reso-

nance imaging of the human brain. *Proc. IEEE*, 84:1488–1496, 1996.
54. S. Geman and D. Geman. Stochastic relaxation, Gibbs distrutions, and the Bayesian restoration of images. *IEEE T. Patt. Anal. Mach. Intel.*, PAMI-6:721–741, 1984.
55. G. Gerig, J. Martin, R. Kikinis, O. Kubler, M. Shenton, and F.A. Jolesz. Unsupervised tissue type segmentation of 3D dual-echo MR head data. *Im. Vis. Comp.*, 29:100–132, 1985.
56. A. Ghanei, H. Soltanian-Zadeh, and J.P. Windham. A 3D deformable surface model for segmentation of objects from volumetric data in medical images. *Computers in Biology and Medicine*, 28:239–253, 1998.
57. P. Gibbs, D.L. Buckley, S.J. Blackband, and A. Horsman. Tumour volume detection from MR images by morphological segmentation. *Phys. Med. Biol.*, 41:2437–2446, 1996.
58. A.F. Goldszal, C. Davatzikos, D.L. Pham, M.X.H. Yan, R.N. Bryan, and S.M. Resnick. An image processing system for qualitative and quantitative volumetric analysis of brain images. *Journal of Computer Assisted Tomography*, 22:827–837, 1998.
59. R.C. Gonzalez and R.E. Woods. *Digital Image Processing.* Addison-Wesley, 1992.
60. C.L. Gordon, C.E. Webber, J.D. Adachi, and N. Christoforou. In vivo assessment of trabecular bone structure at the distal radius from high-resolution computed tomography images. *Phys. Med. Biol.*, 41:495–508, 1996.
61. W.E.L. Grimson, G.J. Ettinger, T. Kapur, M.E. Leventon, W.M. Wells, et al. Utilizing segmented MRI data in image-guided surgery. *Int. J. Patt. Rec. Art. Intel.*, 11:1367–1397, 1997.
62. R. Guillemaud and M. Brady. Estimating the bias field of MR images. *IEEE T. Med. Imag.*, 16:238–251, 1997.
63. R. Gupta and P.E. Undrill. The use of texture analysis to delineate suspicious masses in mammograhy. *Phys. Med. Biol.*, 40:835–855, 1995.
64. L.O. Hall, A.M. Bensaid, L.P. Clarke, R.P. Velthuizen, M.S. Silbiger, and J.C. Bezdek. A comparison of neural network and fuzzy clustering techniques in segmenting magnetic resonance images of the brain. *IEEE T. Neural Networks*, 3:672–682, 1992.
65. P. Hall, M. Ngan, and P. Andreae. Reconstruction of vascular networks using three-dimensional models. *IEEE T. Med. Imag.*, 16:919–929, 1997.
66. R.M. Haralick and L.G. Shapiro. Image segmentation techniques. *Comput. Vis. Graph. Im. Proc.*, 29:100–132, 1985.
67. G.J. Harris, P.E. Barta, L.W. Peng, et al. MR volume segmentation of gray matter and white matter using manual thresholding: dependence on image brightness. *Am. J. Neuroradiol.*, 15:225–230, 1994.
68. S. Haykin. *Neural networks: a comprehensive foundation.* Macmillan College, New York, 1994.
69. T.J. Hebert. Fast iterative segmentation of high resolution medical images. *IEEE T. Nucl. Sci.*, 44:1363–1367, 1997.
70. K. Held, E.R. Kops, B.J. Krause, W.M. Wells, R. Kikinis, et al. Markov random field segmentation of brain MR images. *IEEE T. Med. Imag.*, 16(6), 1997.
71. R.C. Herndon, J.L. Lancaster, A.W. Toga, and P.T. Fox. Quantification of white matter and gray matter volumes from T1 parametric images using fuzzy classifiers. *J. Mag. Res. Imag.*, 6:425–435, 1996.
72. K.H. Hohne and W.A. Hanson. Interactive 3-D segmentation of MRI and CT volumes using morphological operations. *J. Comp. Assist. Tom.*, 16:285–294, 1992.
73. M.A. Hurn, K.V. Mardia, T.J. Hainsworth, J. Kirkbride, and E. Berry. Bayesian fused classification of medical images. *IEEE T. Med. Imag.*, 15:850–858, 1996.
74. N. Ibrahim, H. Fujita, T. Hara, and T. Endo. Automated detection of clustered microcalcifications on mammograms: CAD system application to MIAS database. *Phys. Med. Biol.*, 42:2577–2589, 1997.
75. A.K. Jain and R.C. Dubes. *Algorithms for clustering data.* Prentice Hall, 1988.
76. B. Johnston, M.S. Atkins, B. Mackiewich, and M. Anderson. Segmentation of multiple sclerosis lesions in intensity corrected multispectral MRI. *IEEE T. Med. Imag.*, 15:154–169, 1996.
77. M. Joliot and B.M. Mazoyer. Three-dimensional segmentation and interpolation of magnetic resonance brain images. *IEEE T. Med. Imag.*, 12:269–277, 1993.
78. T.N. Jones and D.N. Metaxas. Segmentation using deformable models with affinity-based localization. *Lecture Notes in Computer Science*, 1205:53–52, 1997.
79. S.C. Joshi, M.I. Miller, and U. Grenander. On the geometry and shape of brain sub-manifolds. *Int. J. Patt. Rec. Art. Intel.*, 11:1317–1343, 1997.
80. V. Juhan, B. Nazarian, K. Malkani, R. Bulot, J.M. Bartoli, and J. Sequeira. Geometrical modelling of abdominal aortic aneurysms. *Lecture Notes in Computer Science*, 1205:243–242, 1997.
81. Y.M. Kadah, A.A. Farag, J.M. Zurada, A.M. Badawi, and A.M. Youssef. Classification algorithms for quantitative tissue characterization of diffuse liver disease from ultrasound images. *IEEE T. Med.*

Imag., 15:466–478, 1996.
82. M. Kallergi, K. Woods, L.P. Clarke, W. Qian, and R.A. Clark. Image segmentation in digital mammography: comparison of local thresholding and region growing algorithms. *Comput. Med. Im. Graph.*, 16:323–331, 1992.
83. M. Kamber, R. Shinghal, D.L. Collins, G.S. Francis, and A.C. Evans. Model-based 3-D segmentation of multiple sclerosis lesions in magnetic resonance brain images. *IEEE T. Med. Imag.*, 14:442–453, 1995.
84. T. Kapur, E. Grimson, W. Wells, and R. Kikinis. Segmentation of brain tissue from magnetic resonance images. *Med. Im. Anal.*, 1:109–127, 1996.
85. T. Kapur, W.E.L. Grimson, R. Kikinis, and W.M. Wells. Enhanced spatial priors for segmentation of magnetic resonance imagery. In *Proc. 1st Int. Conf. Med. Im. Comput. Comp. Assist. Interven. (MICCAI98)*, pages 457–468, 1998.
86. N. Karssemeijer. Automated classification of parenchymal patterns in mammograms. *Phys. Med. Biol.*, 43:365–389, 1998.
87. M. Kass, A. Witkin, and D. Terzopoulos. Snakes: Active contour models. *Int. J. Comp. Vision*, 1:321–331, 1988.
88. J. Kaufhold, M. Schneider, A.S. Willsky, and W.C. Karl. A statistical method for efficient segmentation of MR imagery. *Int. J. Patt. Rec. Art. Intel.*, 11:1213–1231, 1997.
89. N. Khaneja, M.I. Miller, and U. Grenander. Dynamic programming generation of curves on brain surfaces. *IEEE T. Patt. Anal. Mach. Intel.*, 20:1260–1265, 1998.
90. V.S. Khoo, D.P. Dearnaley, D.J. Finnigan, A. Padhani, S.F. Tanner, and M.O. Leach. Magnetic resonance imaging (MRI): considerations and applications in radiotheraphy treatment planning. *Radiother. Oncol.*, 42:1–15, 1997.
91. M.I. Kohn, N.K. Tanna, G.T. Herman, S.M. Resnick, et al. Analysis of brain and cerebrospinal fluid volumes with MR imaging. *Radiology*, 178:115–122, 1991.
92. A. Koivula, J. Alakuijala, and O. Tervonen. Image feature based automatic correction of low-frequency spatial intensity variations in MR images. *Mag. Res. Imag.*, 15:1167–1175, 1997.
93. D. Kucera and R.W. Martin. Segmentation of sequences of echocardiographic images using a simplified 3D active contour model with region based external forces. *Comput. Med. Im. Graph.*, 21:1–21, 1997.
94. M.A. Kupinski and M.L. Giger. Automated seeded lesion segmentation on digital mammograms. *IEEE T. Med. Imag.*, 17:510–517, 1998.
95. D.H. Laidlaw, K.W. Fleischer, and A.H. Barr. Partial-volume bayesian classification of material mixtures in MR volume data using voxel histograms. *IEEE T. Med. Imag.*, 17:98–107, 1998.
96. J.L. Lancaster, L.H. Rainey, J.L. Summerlin, C.S. Freitas, P.T. Fox, A.C. Evans, A.W. Toga, and J.C. Mazziotta. Automated labeling of the human brain: A preliminary report on the development and evaluation of a forward-transform method. *Human Brain Mapping*, 5:238–242, 1997.
97. D.A. Langan, J.W. Modestino, and J. Zhang. Cluster validation for unsupervised stochastic model-based image segmentation. *IEEE T. Im. Process.*, 7:180–195, 1998.
98. S.M. Larie and S.S. Abukmeil. Brain abnormality in schizophrenia: a systematic and quantitative review of volumetric magnetic resonance imaging studies. *J. Psych.*, 172:110–120, 1998.
99. C. Lee, S. Hun, T.A. Ketter, and M. Unser. Unsupervised connectivity-based thresholding segmentation of midsaggital brain MR images. *Comput. Biol. Med.*, 28:309–338, 1998.
100. S.K. Lee and M.W. Vannier. Post-acquisition correction of MR inhomogeneities. *Mag. Res. Med.*, 36:276–286, 1996.
101. F. Lefebvre, G.Berger, and P. Laugier. Automatic detection of the boundary of the calcaneus from ultrasound parametric images using an active contour model: clinical assessment. *IEEE T. Med. Imag.*, 17:45–52, 1998.
102. Tianhu Lei and Wilfred Sewchand. Statistical approach to X-Ray CT imaging and its applications in image analysis – part II: A new stochastic model-based image segmentation technique for X-Ray CT image. *IEEE T. Med. Imag.*, 11(1):62–69, 1992.
103. H. Li, R. Deklerck, B. De Cuyper, A. Hermanus, E. Nyssen, and J. Cornelis. Object recognition in brain CT-scans: knowledge-based fusion of data from multiple feature extractors. *IEEE T. Med. Imag.*, 14:212–229, 1995.
104. H.D. Li, M. Kallergi, L.P. Clarke, V.K. Jain, and R.A. Clark. Markov random field for tumor detection in digital mammagraphy. *IEEE T. Med. Imag.*, 14:565–576, 1995.
105. S.Z. Li. *Markov random field modeling in computer vision.* Springer, 1995.
106. Z. Liang. Tissue classification and segmentation of MR images. *IEEE Eng. Med. Biol.*, pages 81–85, 1993.

107. Z. Liang, J.R. MacFall, and D.P. Harrington. Parameter estimation and tissue segmentation from multispectral MR images. *IEEE T. Med. Imag.*, 13:441–449, 1994.
108. K.O. Lim and A. Pfefferbaum. Segmentation of MR brain images into cerebrospinal fluid and white and gray matter. *J. Comp. Assist. Tom.*, 13:588–593, 1989.
109. Q. Long, X.Y. Xu, M.W. Collins, M. Bourne, and T.M. Griffith. Magnetic resonance image processing and structured grid generation of a human abdominal bifurcation. *Computer Methods and Programs in Biomedicine*, 56:249–259, 1998.
110. A. Macovski. *Medical imaging systems*. Prentice-Hall, 1983.
111. J.B.A. Maintz and M.A. Viergever. A survey of medical image registration. *Med. Im. Anal.*, 2:1–36, 1998.
112. R. Malladi, J.A. Sethian, and B.C. Vemuri. Shape modeling with front propagation: A level set approach. *IEEE T. Patt. Anal. Mach. Intel.*, 17:158–175, 1995.
113. R. Malladi, J.A. Sethian, and B.C. Vemuri. A fast level set based algorithm for topology-independent shape modeling. *Journal of Mathematical Imaging and Vision*, 6:269–289, 1996.
114. J.F. Mangin, V. Frouin, I. Bloch, J. Regis, and J. Lopez-Krahe. From 3D magnetic resonance images to structural representations of the cortex topography using topology preserving deformations. *J. Math. Imag. Vis.*, 5:297–318, 1995.
115. I.N. Manousakas, P.E. Undrill, G.G. Cameron, and T.W. Redpath. Split-and-merge segmentation of magnetic resonance medical images: performance evaluation and extension to three dimensions. *Comput. Biomed. Res.*, 31:393–412, 1998.
116. M.J. McAuliffe, D. Eberly, D.S. Fritsch, E.L. Chaney, and S.M. Pizer. Scale-space boundary evolution initialized by cores. *Lecture Notes in Computer Science*, 1131:173–172, 1996.
117. T. McInerney and D. Terzopoulos. A dynamic finite element surface model for segmentation and tracking in multidimensional medical images with application to cardiac 4D image analysis. *Comput. Med. Im. Graph.*, 19:69–83, 1995.
118. T. McInerney and D. Terzopoulos. Topologically adaptable snakes. In *Proc. Fifth Int. Conf. Comp. Vis.*, pages 840–845, 1995.
119. T. McInerney and D. Terzopoulos. Deformable models in medical image analysis: a survey. *Med. Im. Anal.*, 1:91–108, 1996.
120. T. McInerney and D. Terzopoulos. Medical image segmentation using topologically adaptable surfaces. *Lecture Notes in Computer Science*, 1205:23–22, 1997.
121. M.F. McNitt-Gray, H.K. Huang, and J.W. Sayre. Feature selection in the pattern classification problem of digital chest radiograph segmentation. *IEEE T. Med. Imag.*, 14:537–547, 1995.
122. W. Menhardt and K. Schmidt. Computer vision on magnetic resonance images. *Patt. Rec. Let.*, 8:73–85, 1988.
123. C.R. Meyer, H.B. Peyton, and J. Pipe. Retrospective correction of intensity inhomogeneities in MRI. *IEEE T. Med. Imag.*, 14:36–41, 1995.
124. I. Mikic, S. Krucinski, and J.D. Thomas. Segmentation and tracking in echocardiographic sequences: active contours guided by optical flow estimates. *IEEE T. Med. Imag.*, 17:274–284, 1998.
125. A. Mojsilovic, M.V. Popovic, A.N. Neskovic, and A.D. Popovicq. Wavelet image extension for analysis and classifcation of infarcted myocardial tissue. *IEEE T. Biomed. Eng.*, 44:856–866, 1997.
126. R. Momenan, D. Hommer, R. Rawlings, U. Rutimann, M. Kerich, and D. Rio. Intensity-adaptive segmentation of single-echo T1-weighted magnetic resonance images. *Human Brain Mapping*, 5:194–205, 1997.
127. J. Montagnat and H. Delingette. Volumetric medical images segmentation using shape constrained deformable models. *Lecture Notes in Computer Science*, 1205:13–12, 1997.
128. H.W. Muller-Gartner, J.M. Links, et al. Measurement of radiotracer concentration in brain gray matter using positron emission tomography: MRI-based correction for partial volume effects. *J. Cereb. Blood Flow Metab.*, 12:571–583, 1992.
129. A. Neumann and C. Lorenz. Statistical shape model based segmentation of medical images. *Comput. Med. Im. Graph.*, 22:133–143, 1998.
130. L. Nocera and J.C. Gee. Robust partial volume tissue classification of cerebral MRI scans. In *Proc. of the SPIE Medical Imaging '97: Image Processing*, pages 550–560, 1997.
131. M. Ozkan, B.M. Dawant, and R.J. Micunas. Neural-network based segmentation of multi-modal medical images: a comparative and prospective study. *IEEE T. Med. Imag.*, 12:534–544, 1993.
132. N.R. Pal and S.K. Pal. A review on image segmentation techniques. *Patt. Rec.*, 26:1277–1294, 1993.
133. T.N. Pappas. An adaptive clustering algorithm for image segmentation. *IEEE T. Signal Process.*, 40:901–914, 1992.
134. J.M. Pardo, D.Cabello, and J.Heras. A snake for model-based segmentation of biomedical images.

Patt. Rec. Let., 18:1529–1538, 1997.
135. J.M. Pardo-Lopez, D. Cabello, J. Heras, and J. Couceiro. A Markov random field model for bony tissue classification. *Comput. Med. Im. Graph.*, 22:169–178, 1998.
136. W. Park, E.A. Hoffman, and M. Sonka. Segmentation of intrathoracic airway trees: a fuzzy logic approach. *IEEE T. Med. Imag.*, 17:489–497, 1998.
137. S.D. Pathak, P.D. Grimm, V. Chalana, and Y. Kim. Pubic arch detection in transrectal ultrasound guided prostate cancer therapy. *IEEE T. Med. Imag.*, 17:762–771, 1998.
138. S.D. Pathak, V.Chalana, and Y.M. Kim. Interactive automatic fetal head measurements from ultrasound images using multimedia computer technology. *Ultrasound in Medicine and Biology*, 23:665–673, 1997.
139. T.M. Peters, D.L Collins, and A.C. Evans. Image segmentation and 3-D applications. In *The Physics of MRI: 1992 AAPM Summer School Proceedings*, pages 607–646, 1993.
140. D.L. Pham and J.L. Prince. An adaptive fuzzy c-means algorithm for image segmentation in the presence of intensity inhomogeneities. *Patt. Rec. Let.*, pages 57–68, 1999.
141. D.L. Pham, J.L. Prince, A.P. Dagher, and C. Xu. An automated technique for statistical characterization of brain tissues in magnetic resonance imaging. *Int. J. Patt. Rec. Art. Intel.*, 11(8):1189–1211, 1997.
142. H.H. Pien, M. Desai, and J. Shah. Segmentation of MR images using curve evolution and prior information. *Int. J. Patt. Rec. Art. Intel.*, 11:1233–1245, 1997.
143. S. Pohlman, K.A. Powell, N.A. Obuchowski, W.A. Chilcote, and S. Grundfest-Broniatowski. Quantitative classification of breast tumores in digitzed mamograms. *Med. Phys.*, 23:1337–1345, 1996.
144. W.E. Polakowski, D.A. Cournoyer, SK. Rogers, M.P. DeSimio, D.W. Ruck, J.W. Hoffmeister, and R.A. Raines. Computer-aided breast cancer detection and daignosis of masses using difference of Gaussians and derivative-based feature saliency. *IEEE T. Med. Imag.*, 16:811–819, 1997.
145. C.S. Poon and M. Braun. Image segmentation by a deformable contour model incorporating region analysis. *Physics in Medicine and Biology*, 42:1833–1841, 1997.
146. C.E. Priebe, D.J. Marchette, and G.W. Rogers. Segmentation of random fields via borrowed strength density estimation. *IEEE T. Patt. Anal. Mach. Intel.*, 19:494–499, 1997.
147. J.L. Prince, Q. Tan, and D. Pham. Optimization of MR pulse sequences for Bayesian image segmentation. *Med. Phys.*, 22:1651–1656, 1995.
148. J. Rademacher, A.M Galaburda, D.N. Kennedy, P.A. Filipek, and V.S. Caviness. Human cerebral cortex: localization, parcellation and morphometry with magnetic resonance imaging. *J. Cog. Neuro.*, 4:352–374, 1992.
149. J.C. Rajapakse, J.N. Giedd, and J.L. Rapoport. Statistical approach to segmentation of single-channel cerebral MR images. *IEEE T. Med. Imag.*, 16:176–186, 1997.
150. J.C. Rajapakse and F. Kruggel. Segmentation of MR images with intensity inhomogeneities. *Im. Vis. Comp.*, 16:165–180, 1998.
151. N.C. Andreasen R. Rajarethinam, T. Cizadlo, et al. Automatic atlas-based volume estimation of human brain regions from MR images. *J. Comp. Assist. Tom.*, 20:98–106, 1996.
152. W.E. Reddick, J.O. Glass, E.N. Cook, T.D. Elkin, and R.J. Deaton. Automated segmentation and classification of multispectral magnetic resonance images of brain using artificail neural networks. *IEEE T. Med. Imag.*, 16:911–918, 1997.
153. T.R. Reed and J.M. Hans Du Buf. A review of recent texture segmentation and feature extraction tecniques. *CVGIP: Im. Understand.*, 57:359–372, 1993.
154. A.L. Reiss, J.G. Hennessey, M. Rubin, L. Beach, M.T. Abrams, et al. Reliability and validity of an algorithm for fuzzy tissue segmentation of MRI. *J. Comp. Assist. Tom.*, 22:471–479, 1998.
155. P.K. Sahoo, S. Soltani, and A.K.C. Wong. A survey of thresholding techniques. *Comput. Vis. Graph. Im. Proc.*, 41:233–260, 1988.
156. S. Sandor and R. Leahy. Surface-based labeling of cortical anatomy using a deformable atlas. *IEEE T. Med. Imag.*, 16:41–54, 1997.
157. P. Santago and H.D. Gage. Quantification of MR brain images by mixture density and partial volume modeling. *IEEE T. Med. Imag.*, 12:566–574, 1993.
158. P. Santago and H.D. Gage. Statistical models of partial volume effect. *IEEE T. Image Process.*, 4:1531–1540, 1995.
159. R.J. Schalkoff. *Pattern recognition: statistical, structural and neural approaches.* John Wiley and Sons, 1992.
160. A. Sebbahi, A. Herment, A. deCesare, and E. Mousseaux. Multimodality cardiovascular image segmentation using a deformable contour model. *Comput. Med. Im. Graph.*, 21:79–89, 1997.
161. J. Sijbers, P. Scheunders, M. Verhoye, A. Van Der Linden, D. Van Dyck, et al. Watershed-based

segmentation of 3D MR data for volume quantization. *Mag. Res. Imag.*, 15:679–688, 1997.
162. A. Simmons, P.S. Tofts, G.J. Barker, and S.R. Arridge. Sources of intensity nonuniformity in spin echo images at 1.5T. *Mag. Res. Med.*, 32:121–128, 1994.
163. H.R. Singleton and G.M. Pohost. Automatic cardiac MR image segmentation using edge detection by tissue classification in pixel neighborhoods. *Mag. Res. Med.*, 37:418–424, 1997.
164. J.G. Sled and G.B. Pike. Standing-wave and RF penetration artifacts caused by elliptic geometry: an electrodynamic analysis of MRI. *IEEE T. Med. Imag.*, 17:653–662, 1998.
165. J.G. Sled, A.P. Zijdenbos, and A.C. Evans. A nonparametric method for automatic correction of intensity nonuniformity in MRI data. *IEEE T. Med. Imag.*, 17:87–97, 1998.
166. H. Soltanian-Zadeh, J.P. Windham, and D.J. Peck. Optimal linear transformation for MRI feature extraction. *IEEE T. Med. Imag.*, 15:749–767, 1996.
167. M. Sonka, W. Park, and E.A. Hoffman. Rule-based detection of intrathoracic airway trees. *IEEE T. Med. Imag.*, 15:314–326, 1996.
168. M. Sonka, M.D. Winniford, and S.M. Collins. Robust simultaneous detection of coronary borders in complex images. *IEEE T. Med. Imag.*, 14:151–161, 1995.
169. M. Sonka, X. Zhang, M. Siebes, M.S. Bissing, S.C. DeJong, S.M Collins, and C.R. McKay. Segmentation of intravascular ultrasound images: a knowledge-based approach. *IEEE T. Med. Imag.*, 14:719–732, 1995.
170. P. Sprawls. *Physical principles of medical imaging*. Aspen Publishers, 1993.
171. R.N. Strickland and H.I. Hahn. Wavelet transforms for detecting microcalcifcations in mammograms. *IEEE T. Med. Imag.*, 15:218–229, 1996.
172. P. Suetens, E. Bellon, D. Vandermeulen, M. Smet, G. Marchal, J. Nuyts, and L. Mortelmans. Image segmentation: methods and applications in diagnostic radiology and nuclear medicine. *Eur. J. of Radiology*, 17:14–21, 1993.
173. G. Szekely, A. Kelemen, C. Brechbuhler, and G. Gerig. Segmentation of 2-D and 3-D objects from MRI volume data using constrained elastic deformations of flexible Fourier contour and surface models. *Med. Im. Anal.*, 1:19–34, 1996.
174. Y.C. Tai, K.P. Lin, M. Dahlbom, and E.J. Hoffman. A hybrid attenuation correction technique to compensate for lung density in 3-D total body PET. *IEEE Trans. on Nuclear Science*, 43:323–330, 1996.
175. J. Talairach and P. Tournoux. *Co-Planar Stereotaxic Atlas of the Human Brain. 3-Dimensional Proportional System: An Approach to Cerebral Imaging*. Thieme Medical Publisher, Inc., Stuttgart, NY, 1988.
176. P. Taylor. Invited review: computer aids for decision-making in diagnostic radiology— a literature review. *Brit. J. Radiol..*, 68:945–957, 1995.
177. H. Tek and B.B. Kimia. Volumetric segmentation of medical images by three-dimensional bubbles. *Comp. Vis. Im. Understand.*, 65:246–258, 1997.
178. P.C. Teo, G. Sapiro, and B.A. Wandell. Creating connected representations of cortical gray matter for functional MRI visualization. *IEEE T. Med. Imag.*, 16:852–863, 1997.
179. Y. Zimmerand R. Tepper and S. Akselrod. A two-dimensional extension of minimum cross entropy thresholding for the segmentation of ultrasound images. *Ultrasound Med. Biol.*, 22:1183–1190, 1996.
180. D. Terzopoulos and R. Szeliski. Tracking with Kalman snakes. In A. Blake and A. Yuille, editors, *Active Vision*, Artificial Intelligence, pages 3–20. The MIT Press, Cambridge, Massachusetts, 1992.
181. P. Thompson and A.W. Toga. Detection, visualization and animation of abnormal anatomic structure with a probabilistic brain atlas based on random vector field transformations. *Med. Im. Anal.*, 1:271–294, 1997.
182. C. Tsai, B.S. Manjunath, and R. Jagadeesan. Automated segmentation of brain MR images. *Patt. Rec.*, 28:1825–1837, 1995.
183. J. K. Udupa and S. Samarasekera. Fuzzy connectedness and object definition: Theory, algorithms and applications in image segmentation. *Graph. Mod. Im. Proc.*, 58(3):246–261, 1996.
184. J.K. Udupa and G.T. Herman, editors. *3-D Imaging in Medicine.* CRC Press, 1991.
185. J.K. Udupa, L. Wei, S. Samarasekera, Y. Miki, M.A. van Buchem, and R.I. Grossman. Multiple sclerosis lesion quantification using fuzzy-connectedness principles. *IEEE T. Med. Imag.*, 16:598–609, 1997.
186. M. Vaidyanathan, L.P. Clarke, L.O. Hall, C. Heidtman, R. Velthuizen, et al. Monitoring brain tumor response to therapy using MRI segmentation. *Mag. Res. Imag.*, 15:323–334, 1997.
187. M. Vaidyanathan, L.P. Clarke, R.P. Velthuizen, S. Phuphanich, A.M. Bensaid, et al. Comparison of supervised MRI segmentation methods for tumor volume determination during therapy. *Mag. Res. Imag.*, 13:719–728, 1995.

188. D. Vandermeulen, R. Verbeeck, L. Berben, D. Delaere, P. Suetens, and G. Marchal. Continuous voxel classification by stochastic relaxation: theory and application to MR imaging and MR angiography. *Im. Vis. Comp.*, 12:559–572, 1994.
189. M.W. Vannier, R.L. Butterfield, et al. Multispectral analysis of magnetic resonance images. *Radiology*, 154:221–224, 1985.
190. B.C. Vemuri, Y. Guo, C.M. Leonard, and S. Lai. Fast numerical algorithms for fitting multiresolution hybrid shape models to brain MRI. *Med. Im. Anal.*, 1:343–362, 1997.
191. D.L. Vilarino, V.M. Brea, D. Cabello, and J.M. Pardo. Discrete-time CNN for image segmentation by active contours. *Patt. Rec. Let.*, 19:721–734, 1998.
192. L. Vincent and P. Soille. Watersheds in digital spaces: an efficient algorithm based on immersion simulation. *IEEE T. Patt. Anal. Mach. Intel.*, 13:583–598, 1991.
193. N.F. Vittitoe, R. Vargas-Voracek, and C.E. Floyd. Identification of lung regions in chest radiographs using Markov random field modeling. *Med. Phys.*, 25:976–985, 1998.
194. Y. Wang, T. Adah, and S. Kung ad Z. Szabo. Quantification and segmentation of brain tissues from MR images: a probabilistic neural network approach. *IEEE T. Im. Process.*, 7:1165–1181, 1998.
195. Y. Wang and L.H. Staib. Boundary finding with correspondence using statistical shape models. In *Proc. IEEE Conf. Comp. Vis. Patt. Rec.*, pages 338–345, 1998.
196. S. Warfield, J. Dengler, J. Zaers, C.R.G. Guttmann, W.M. Wells, et al. Automatic identification of grey matter structures from MRI to improve the segmentation of white matter lesions. *Journal of Image Guided Surgery*, 1(6):326–338, 1995.
197. W.M. Wells, W.E.L. Grimson, R. Kikins, and F.A. Jolesz. Adaptive segmentation of MRI data. *IEEE T. Med. Imag.*, 15:429–442, 1996.
198. A.J. Worth, N. Makris, V.S. Caviness, and D.N. Kennedy. Neuroanatomical segmentation in MRI: technological objectives. *Int. J. Patt. Rec. Art. Intel.*, 11:1161–1187, 1997.
199. P. Wust, J. Gellermann, J. Beier, S. Wegner, W. Tilly, et al. Evaluation of segmentation algorithms for generation of patient models in radiofrequency hyperthermia. *Phys. Med. Biol.*, 43:3295–3307, 1998.
200. C. Xu, D.L. Pham, J.L. Prince, M.E. Etemad, and D. Yu. Reconstruction of the central layer of the human cerebral cortex from MR images. In *Proc. 1st Int. Conf. Med. Im. Comput. Comp. Assist. Intervent.*, pages 482–488, 1998.
201. C. Xu and J.L. Prince. Snakes, shapes, and gradient vector flow. *IEEE T. Im. Process.*, 7:359–369, 1998.
202. M.X.H. Yan and J.S. Karp. An adaptive Bayesian approach to three-dimensional MR brain segmentation. In *Proc. of XIVth International Conference on Information Processing in Medical Imaging*, pages 201–213, 1995.
203. A. Yezzi, S. Kichenassamy, A. Kumar, P. Olver, and A. Tannenbaum. A geometric snake model for segmentation of medical imagery. *IEEE T. Med. Imag.*, 16:199–209, 1997.
204. Z. Yue, A. Goshtasby, and L.V. Ackerman. Automatic detection of rib borders in chest radiographs. *IEEE T. Med. Imag.*, 14:525–536, 1995.
205. L.A. Zadeh. Fuzzy sets. *Information and Control*, 8:338–353, 1965.
206. Y.J. Zhang. A survey on evaluation methods for image segmentation. *Patt. Rec. Let.*, 29:1335–1346, 1996.
207. Y. Zhu and H. Yan. Computerized tumor boundary detection using a hopfield neural network. *IEEE T. Med. Imag.*, 16:55–67, 1997.
208. A.P. Zijdenbos and B.M. Dawant. Brain segmentation and white matter lesion detection in MR images. *Critical Reviews in Biomedical Engineering*, 22:401–465, 1994.